Materials and Design 190 (2020) 108580

Contents lists available at ScienceDirect

Materials and Design

journal homepage: www.elsevier.com/locate/matdes

The challenge of upscaling paraffin wax actuators

Arne Mann, Thiemo Germann *, Mats Ruiter, Peter Groche *

Institute for Production Engineering and Forming Machines, Technische Universität Darmstadt, Germany

HIGHLIGHTS

- Presentation of a new concept of powerful phase change actuators in membrane design
- Description of the manufacturing method and challenges of the joining process
- Characterization shows actuating forces of up to 65 kN with high reproducibility
- Compared to existing systems with similar working principle systems, the working density is increased by a factor of 7
- Demonstrator application with passive actuator, compensating the loss of pretension due to thermal loads of a bolted joint

GRAPHICAL ABSTRACT

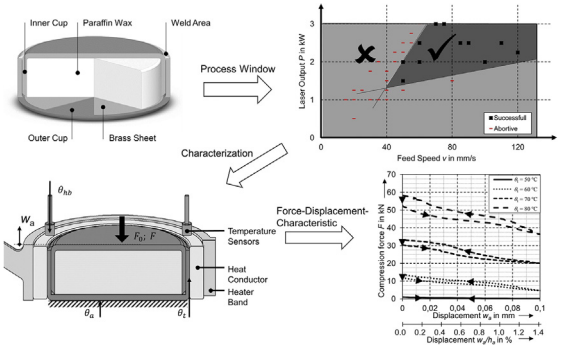

ARTICLE INFO

Article history:
Received 23 November 2019
Received in revised form 14 February 2020
Accepted 17 February 2020
Available online xxxx

Keywords:
Paraffin wax
Actuator
Phase change material
Machinery property adjustment
Automation

ABSTRACT

Higher levels of automation necessitate active spacer and adjusting elements generating high stroke forces. For these, the multitude of applications inside a manufacturing system requires a space- and cost-effective design. Conventional actuator concepts struggle with these demands. A new and efficient actuator concept for establishing closed-loop control circuits is needed. This article presents a new actuator concept, based on the phase change material paraffin wax. Although paraffin wax actuators are a convenient solution for microactuators, high force macroscopic actuators are not established yet. On a macroscopic scale the design of the actuator housing and the manufacturing process are challenging. The presented concept consists of a closed housing, which surrounds the phase change material. A compact actuator design without sealed moveable parts is realized. Thus, the actuators provide high axial forces. Compared to existing solutions an increase in performance by a factor of 7 could be achieved. The essential actuator structure is introduced, characterized and the challenges in manufacturing are discussed. A possible application is demonstrated by a thermal compensation element activated by energy from the surroundings.

1. Introduction

Smaller batches as well as shorter delivery and manufacturing times require a continuous innovation of the manufacturing technologies. Currently, industry 4.0 and the consequent digitalization of the industrial plants are promising approaches for higher level manufacturing systems [1]. More and more manufacturing processes are equipped

* Corresponding authors.
E-mail addresses: germann@ptu.tu-darmstadt.de (T. Germann), groche@ptu.tu-darmstadt.de (P. Groche).

https://doi.org/10.1016/j.matdes.2020.108580

with sensor systems [2]. Process information is recorded and the collected data can contribute to an improved process understanding based on white or grey box models [3]. The next step in manufacturing research is using the deeper process understanding and the determined cause and effect relationships to establish controlled manufacturing processes, as shown by Alwood et al. [4]. The objective of automation at this level is to control product features with a closed loop control [5].

Several different actuator principles have been implemented in closed loop control circuits for the main drives as well as the auxiliary drives used for clamping and adjustment operations. For main drives in machine tools, actuators using hydraulic, pneumatic or electric drives are well established. In contrast, attractive and economical actuator concepts for auxiliary drives (optional process drive for e.g. automatization or adjustment) seem to be of short supply. Fig. 1 shows a classification of actuator tasks in dependency on the process' main drive actuation speed. Applications with the need for higher speeds are often necessary to counteract the impact of stochastic process disturbances. Examples of stochastic disturbances are fluctuating material properties or states of lubrication. In these cases, a rapid process adjustment is required. Countermeasures initiated by actuators may lead to a direct compensation of the process deviations or a compensation in a following process step using closed loop or feed forward controls [4].

Since they also render manually operated machinery adjustments unnecessary, higher levels of automation in manufacturing [4] need control circuits beyond closed loop control of main drives. The targeted adjustment actuations of machine parameters are carried out with an actuating speed below the process cycle frequency (Fig. 1). The main cause for necessary machinery adjustments is given by gradual shifts in system properties. Examples can be the repositioning of a tool that no longer generates the target geometry of a component due to wear. The auxiliary drives may also compensate the deflection of deep drawing tools [6], setting the guiding clearance or adjusting the tool mounting condition [7]. Other examples are process shifts due to thermal expansion of machine components or deterioration of the fluid media's mechanical properties [8]. For this kind of application with low actuation speeds and power requirements, the actuators must be able to provide forces of several kilonewtons whereas typically small displacements in the millimetre range and reaction times of several seconds are sufficient.

In the field of manufacturing process control, thermal expansion is yet an uncommon actuator principle. It seems however promising, especially when phase change materials are used. According to Ogden et al., who compared the energy densities of different actuator materials, phase change materials have the highest energy density compared to shape memory alloys, electromagnetic, thermopneumatic, bimetallic, electrostatic and piezoelectric actuator materials (Fig. 2). The high energy density is due to the high thermal expansion coefficient combined with a low compressibility [9]. A drawback of thermal actuators which is counteracting the common use in manufacturing processes is their low

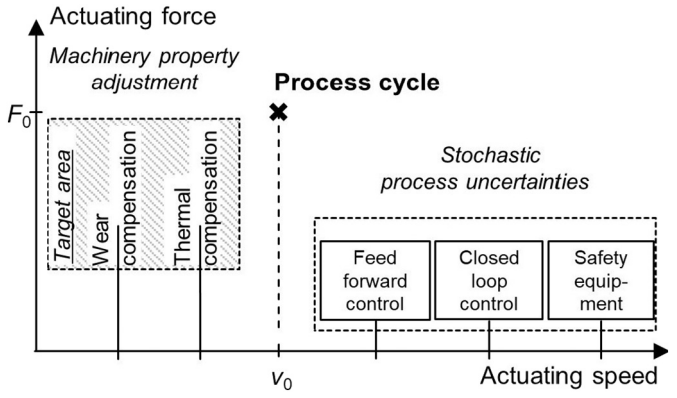

Fig. 1. Overview of necessary actuator dynamics for different applications in manufacturing industry.

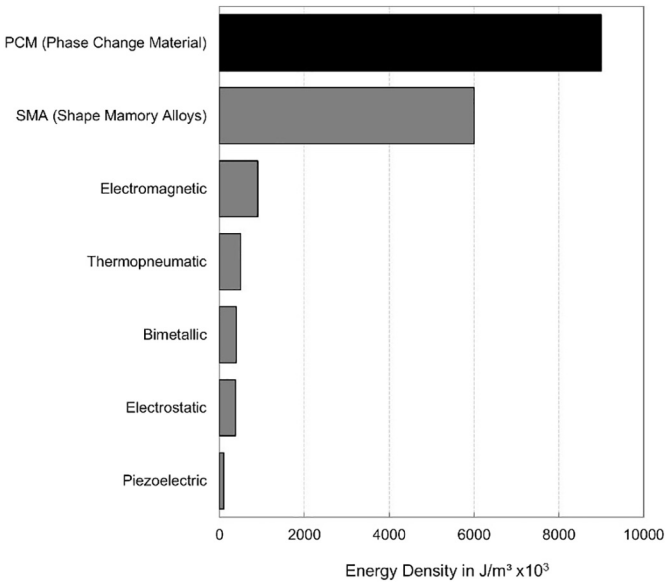

Fig. 2. Energy density of different actuator materials (adapted by the author) [10].

energy efficiency. However, by using the lost heat of processes or machines, the low-efficiency of the thermal actuators is of minor importance.

The selected material for this investigation is paraffin wax. Paraffin wax is a phase change material, which has a significant volume increase when changing from solid to liquid state. Its small compressibility qualifies it to be an especially suited phase change material. Paraffin wax is activated by applying heat [10]. For instance, the paraffin wax used in this publication (SIGMA-ALDRICH paraffin wax mp 58–62 °C) shows a free volume expansion of approximately 15% at 75 °C compared to 25 °C [11]. The activation time depends on the time required for heat supply to and distribution within the paraffin wax. The low thermal conductivity of the paraffin wax (0.21 W/mK [12]) leads to a rather inert actuator behaviour. This means for short response times, e.g. for process adjustments (compare Fig. 1), the amount of paraffin is to be kept low (miniaturized actuators). Additionally the thermal conductivity can be increased by additives [13], enabling faster response times.

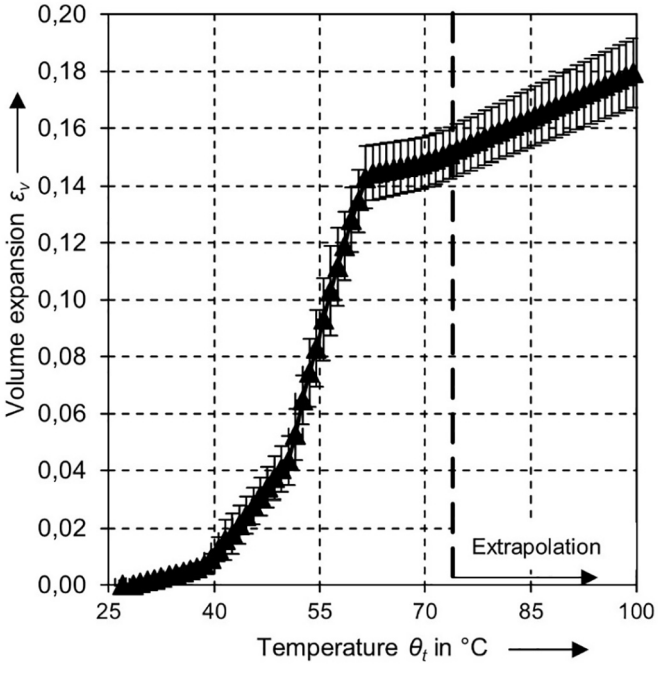

Fig. 3. Volume expansion data of SIGMA-ALDRICH paraffin wax mp 58–62 °C [11].

For current actuator designs, there are different options to convert the expansion of the phase change material into a force transmission. Ogden et al. divide the possible mechanical transmission elements in pistons, membranes, composites and direct contact [10]. Today paraffin wax is commonly used for miniaturized phase change actuators.

Another field of application of paraffin wax is the integration as a functional material in smart structures. Recent examples are temperature responsive surfaces, which enable for passive and active droplet motion control as well as anti-fogging control on miscellaneous surfaces. The paraffin wax determines the slipperiness of the material by its temperature dependent structure [14]. The thermal properties of paraffin wax are furthermore employed in realizing artificial muscles. Their ability to wet carbon nanotubes leads to the use as thermal activated fibers [15]. Further investigations show the high potential of tailored fillers by blending paraffin wax with other polymers [16]. An overview of the current research of twisted nanofibers is provided by Mirvakili and Hunter [17]. Another approach is the use of the paraffins volume expansion as McKibben muscles. A tailored braid of intertwined steel and cotton with a paraffin filling generates a contraction by heating the paraffin wax [18].

Nevertheless the first applications of paraffin wax known to the authors were used as temperature sensitive closures in sealing means [19]. Today's often employed macroscopic paraffin actuators based on a piston design can be ascribed to Sherwood, who invented the electrically heated paraffin wax actuator in the 1960s [20].

The use of a piston is known from hydraulics and pneumatics. Inside piston-cylinder systems, relative movements between the piston and the cylinder take place due to a change of volume in the chamber between piston and cylinder. The contact area between cylinder and piston has the function of sealing the active fluid media and often also of guiding the piston during its movement. In this application, ring seals are often used. Tibbitts presents a commonly used cylinder piston design for a paraffin wax actuator [21]. In comparison with the actuator concepts described above, the actuator housing is significantly larger. The cylindrical housing has a length of 58 mm and a stroke of 25 mm, whereby the paraffin chamber is sealed with an O-ring fixed with a screw thread. The actuator reaches a maximum force of 160 N. Another cylinder piston design actuator presented by Kabei et al. has a paraffin chamber length of 90 mm and a diameter of 2 mm [22]. The paraffin is sealed in a silastic tube. Under free expansion the actuator reaches a maximum stroke between 9 and 10 mm, which decreases slightly under a load of $m = 1000$ g. The subsequently presented patent describes the commercially used actuator design. The cylinder-piston actuator design is similar to the one proposed by Kabei et al., which seals the paraffin with a membrane or an elastomer insert [23]. The housing is joined by a mechanical bond. The actuator reaches a maximum force of 1500 N. During the design of such a system, the sealing technology and the loads during use are important design criteria, as the sealing and guiding function can only be maintained within narrow geometric tolerances. Since the cylinder is designed as an open component, the necessary stiffness must be generated by a large wall thickness. In conclusion, the cylinder-piston system seems to be complex, although the piston design can realize large forces and large displacements at the same time. In addition to ring seals, membranes are used in piston-cylinder paraffin actuators for sealing the cylinder [23].

Using a membrane design, the membrane seals the paraffin wax in a cavity and deflects during an actuator stroke. Since the amount of paraffin significantly determines the response behavior of the actuators, paraffin wax phase change actuators with larger membrane designs are uncommon today. The maximum force of actuators with a membrane is determined, among other factors, by the properties of the membrane and its bonding to the paraffin cavity. The force transmission and the displacement are caused by an elastic deformation of the membrane. The achievable maximum force limits the usage to specific applications as valves and pumps [10]. The operating behaviour of an actuator in membrane design results by the interaction of the individual system components.

The use of phase change materials within microactuators, mircopumps and microvalves is quite common. Due to the high energy density and the good availability, paraffin wax is often the chosen material. Typically, the paraffin wax is encapsulated within a solid housing with a flexible part, e.g. a membrane, to apply the actuation [10]. In a review paper Ogden et al. describe three material classes, which are typically used for microscopic phase change actuators (compare Fig. 4). The most common design in microfabrication bases on silicon and glass. They both exhibit high stiffness and yield strength, which predestines them for high-force or high-pressure applications. A strong sealing was achieved with anodic bonding or fusion of different layers. Examples are the concept of Klintberg et al. [24,25] or Carlen and Mastrangelo [26]. Alternatively, polydimethylsiloxane PDMS or polymers in general are employed. Their advantage lies in simple processing and, for polymers, high stiffness as well as yield strength. This design is typical for microvalves and micropumps as shown in Bóden et al. [27] or Svenson et al. [28]. The third material class consists of metals, especially stainless steels. It is characterized by appropriate high mechanical properties but exhibits difficulties if a direct bonding is targeted. Typically, a polymeric bonding agent is used as an intermediate layer [10]. Examples are summarized by Ogden et al. [10] or Lehto [29].

Despite the described challenges, there are macroscopic actuator designs, which are commonly used today. A typical application of macroscopic paraffin wax actuators are thermostatic working elements such as thermal switches and mixing taps [10]. These actuators in piston design can achieve high displacements, but they have restricted maximum forces. Due to the typical usage as thermostatic working elements, a maximum force was not specified as a target development parameter [30]. Thereby those approaches are not sufficient for the presented application, i.e. adjusting machinery properties (compare Fig. 1), since it requires a high stroke force of several kilonewton.

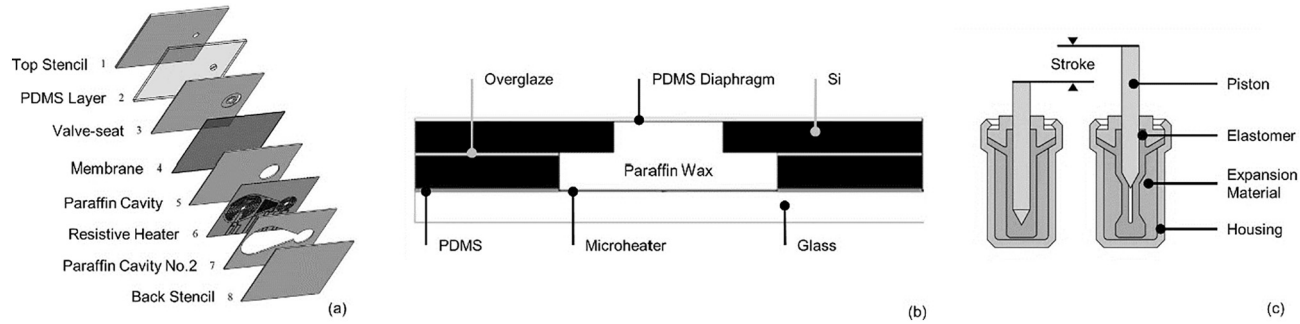

Fig. 4. Different types of paraffin actuators: Polymer stencil design (a) [10], silicon glass design (b) [31], piston design (c) [23] (graphics adapted).

To evaluate the efficiency of the presented actuator concepts a comparative figure is needed. Introducing the work density, Krulevitch et al. enable a useful comparison between different types and sizes of actuators. It is defined as the work output per unit volume W_d [32]. It is defined by the filling volume V, the maximum deflection d_{max} and the actuating force at this point F_{max}.

$$W_d = \frac{F_{max} d_{max}}{2} \frac{1}{V} \tag{1}$$

Ogden et al. presented a comparison of known actuator concepts. Summarising the investigation results, the commonly used membrane design actuators achieve a work density between $7.2 * 10^3\ J/m3$ [33] and $93 * 10^3\ J/m3$ [34]. Due to the stiffer structure of the housing within a piston design, the achievable work density is considerably higher ($260 * 10^3\ J/m3$ [30]). Still, there is a gap by an order of magnitude between current actuators and the potential of paraffin wax (compare Fig. 2). Therefore, upscaling the structure of microactuators is a promising approach.

The objective of this research is to realize a macroscopic paraffin wax actuator for high axial forces. An upscaling of the silicon glass design is not feasible due to process limits of anodic bonding even though the high stiffness and yield strength provide the necessary basis for macroscopic actuators. Therefore, PDMS actuators are no applicable solutions, as their housing stiffness is not sufficient for the intended force range of the actuator. The third housing material class defined by Ogden et al. is metal. The material properties of the metal housing might be promising. However, since the design target of piston actuators are high displacements, whereas the stroke force is subordinated, the piston design is not sensible for upscaling [30]. Another design is an actuator structure out of a stack of metal stencils and polyimide foils, which creates a very high stiffness. Therefore, this design is e.g. the one of choice for micropumps [34]. However, upscaling this design to utilize a macroscopic amount of paraffin wax results in an inapplicable housing. Therefore, a new approach is necessary to design a macroscopic phase change actuator which provides high actuation forces within a relatively small displacement and limited housing space.

This study presents a new design of macroscopic phase change material actuators, which provides solutions for the addressed application.

2. The closed laser-welded phase change material actuator

Based on the aforementioned application areas the requirements of a targeted paraffin actuator can be defined. In order to affect the properties of manufacturing machines, a sufficient actuation force is the most important parameter. Compared to that, a short reaction time is of less importance (compare Fig. 1). The compensation of geometrical changes due to thermal stress or wear requires a high stiffness of the actuator, though the displacement can be rather small [8].

Under the described boundary conditions, the membrane principle appears to be promising. Due to the closed design, the maximum forces are limited by the used materials and joining technologies. The design presented below is intended to withstand high internal pressures due to a closed sheet metal housing and a metallurgical high-strength joint created through laser welding.

Fig. 5 illustrates the design of the phase change actuator concept for high forces. The design of the described actuator concept is mainly affected by the necessity to implement a metallurgical bond to join the housing. Through the metallurgical bond, the housing withstands the working pressure and a sealing of the housing is guaranteed. The realization of the bonding by laser welding minimizes the amount of heat applied. Still the housing needs to be sealed during the welding process, due to the increasing pressure resulting from the heat transfer from the weld area into the paraffin wax. For this reason, a cutting seal is included in the actuator housing design.

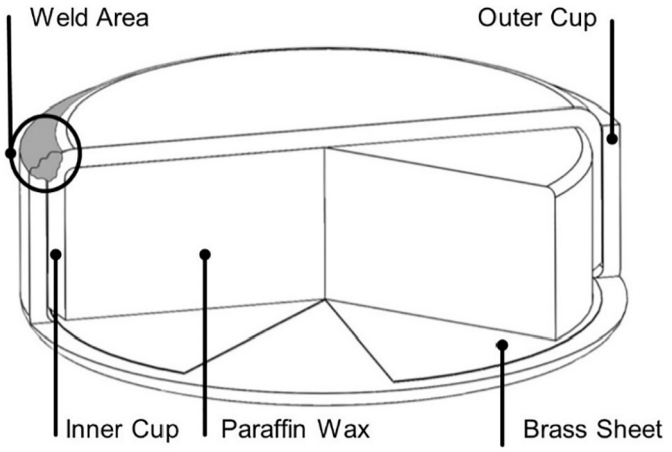

Fig. 5. Design of the phase change actuator in a cross-sectional view.

The setup of the actuator is axisymmetric and consists of two deep drawn cups (inner and outer cup) with the target geometrical dimensions defined in Table 1. The cup diameters are designed to ensure that the inner cup fits into the outer cup. For each cup, specific deep drawing tools are implemented and the steel grade DP600 with thickness of 1 mm is used. A hydraulic press realizes the deep drawing process during which an additional counter punch for a plane cup bottom is applied. The deep drawing process is followed by a turning process, which reduces the cup height to a constant height all over the perimeter. At the inner cup's tip, a chamfer is positioned. The inner cup is filled with liquid paraffin wax (SIGMA-ALDRICH paraffin wax mp 58–62 °C). During the cooling-down, additional paraffin wax is poured into the cup to compensate the lacking volume in the cup due to shrinkage. Filling the actuator in its entirety is achieved by a continuous refill up to a surplus. At the end of the filling process, excess paraffin wax above the cup edge is removed. Inside the outer cup, a brass sheet is placed (thickness 50 μm). Both cups have a fixed height, which leads to a weld area between the outer cup's tip and the radius of the inner cup (Fig. 5). Between both cups results a contact line at the inner cup's tip and the outer cups bottom, which is positioned opposite to the weld area and represents the sealing. Due to an axial force during the joining process, the chamfer of the inner cup cuts into the brass sheet and establishes a sealing function as a cutting seal. The axial force can control the bearable sealing pressure. Both cups are joined by welding.

The welding of the filled actuator cups described in this paragraph is the most critical part of the production chain. For the welding process, an YLS-300-S2T laser source with 3 kW maximum output is used. For a positive outcome of the welding process, the key parameter is the energy per unit length. Due to the round shape of the actuators, a stationary welding point is combined with a rotating clamping of the actuator. The feed speed is defined by the rotations per second and the shape of the actuator. Still there are various other parameters to adjust as the focus position, the welding angle or the axial locking force. The energy per unit length is discussed in detail while the other parameters have been fixed as shown in Table 2; the results are shown in Fig. 6.

Table 1
Geometric parameters of the actuator housing

	Inner cup (I)	Outer cup (O)
Diameter d_i in mm	27.00	28.75
Thickness bottom t_b in mm	1.00	1.00
Thickness wall t_w in mm	0.80	0.80
Radius r_I, r_O in mm	1.00	0.50
Material [−]	DP600	DP600

Table 2
Process parameters of the laser welding process of the actuator housing.

Process parameter	
Welding angle in °	30.0
Axial locking force in kN	2.0
Paraffin wax filling volume in %	99.0
Diameter weld spot in mm	1.2
Overlap weld seam in %	0.75

The process window describe by the energy per unit length is characterized by three typical cases (compare Fig. 6). The first is defined with an insufficient energy per unit length. It occurs when the feed speed is high in relation to the laser power. The outcome is an unsteady weld seam, which only partly joins the components. This unsteady weld seam is due to an insufficient weld pool, either the inner or the outer cup is not sufficiently melted. Predominantly, the outer cup shows a molten edge, whereas the inner cup is not affected. If the energy per unit length is too high, the resulting weld seams are equally unacceptable. This second case can be subdivided in three cases by the increasing laser power (compare Fig. 6). If a low laser power and feed speed is used, the process time is long enough for the paraffin to build up a significant amount of liquid phase. The resulting volume expansion lifts the cups of the actuator against the axial locking force. Therefore, liquid paraffin wax emerges and inhibits the welding. Contrary a very high laser output effects an immediate spraying of the paraffin through the molten actuator cups. This effect results from a local pressure increase at the weld line due to the high amount of applied heat. After the solidification the weld seam still shows points of separation. With a medium high laser power hybrid forms of both processes where detectable. The third case is the right relation of feed speed and laser power. In this situation strong weld seams are achievable. Case 3 in Fig. 6 defines the process window for the manufacturing of macroscopic paraffin wax actuators.

3. Experimental characterization of the phase change actuator

In the following section an examination procedure for the characterization of the novel actuator is presented. Therefore, the used test setup and test cycle are explained. It is used for the determination of achievable forces. Additionally, a force-displacement characterization will be discussed. Subsequently the hysteresis behaviour is characterized. Since the material behaviour of paraffin wax is strongly temperature-depended four different temperatures close to the melting point are considered for the characterization.

The examination takes place in a combined tensile compression test machine (Zwick Roell 100) using an upsetting tool for applying a compression force F to the actuators top and bottom contact area. During the heating, the positions of both pressure plates are fixed by an optical path control, which prevents axial movements. The resulting axial compression force F is recorded. Due to the optical measurement at the upper and lower pressure plate, the mechanical compliance of the test machine is negligible, as a repeatable testing with a pre force of $F_0 = 500$ N is applied prior to the heating. A heater band (270 W; 86.12 mW/mm2) is used to heat the actuator around its housing shell (compare Fig. 7). The target temperature θ_t is set and the heater band is powered continuously until the target temperature is reached. The temperature is kept at the target temperature θ_t by a control for the heating interval t_h. The control temperature for the target temperature θ_t is measured between heater band and actuator housing in an additional aluminum ring serving as heat conductor and sensor mount. The ring includes three evenly distributed thermocouples. The average temperature of these thermocouples is labelled as the heater band temperature θ_{hb} and is used as a feedback signal in the closed loop control. The aluminum ring is slotted to prevent a radial support of the actuator. An additional thermocouple is placed at the bottom centre of the actuator and measures the actuator temperature θ_a.

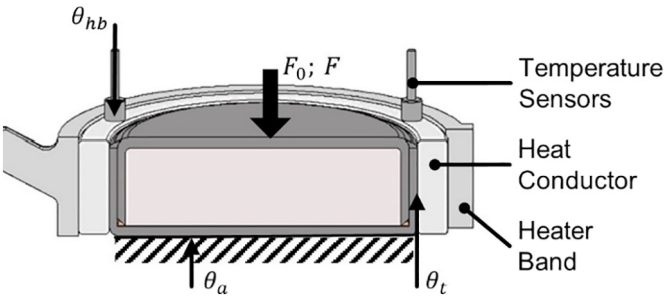

Fig. 7. Structure of the test bench and measuring points of the parameters.

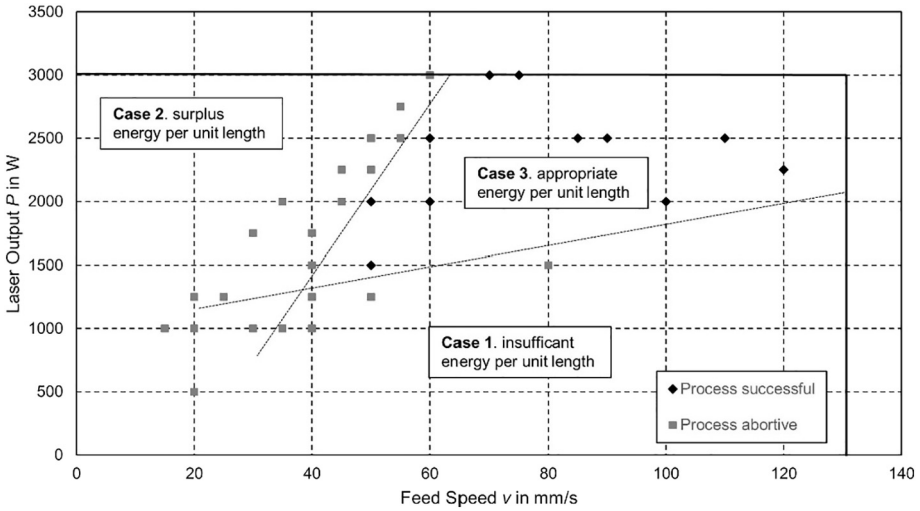

Fig. 6. Process window of the actuator manufacturing according to the energy per unit length.

The tested target temperatures θ_t are $\theta_t = 50$ °C, 60 °C, 70 °C, 80 °C. Each temperature trial consists of four cycles. Hereby, each temperature trial for a fixed actuator height and temperature consists out of four heating and cooling intervals. Fig. 8 exemplifies the testing procedure. Every temperature trial consists of the target temperature θ_t, the heating interval t_h, the cool down temperature θ_c and the number of repetitions n ($n = 4$). The experimental characterization starts at room temperature. At first, the heater band temperature θ_{hb} is set to the cool down temperature θ_c. After reaching the cool down temperature, the heater band temperature is set to the target temperature and the characterization starts. The heating lasts for $t_h = 1200$ s.

Fig. 8 shows an increasing heater band temperature θ_{hb}, which oscillates above the target temperature θ_t. After the heating phase, the free cooling starts. When the cooling temperature θ_c is reached, the next cycle starts at this point.

A complete characterization procedure of an actuator with the compression force F and the actuator temperature θ_t is presented in Fig. 9. The target temperatures θ_t are tested one after the other ($\theta_t = 50$ °C, 60 °C, 70 °C, 80 °C). Each target temperature is set four times. The complete experimental characterization took place over a period of about 11.5 h, for the sake of clarity the experimental progress is given instead of the time.

At the beginning, the target temperature leaps to $\theta_t = 50$ °C. Fig. 9 shows the corresponding actuator temperature θ_a. The test setup consists of highly heat conductive parts, therefore a temperature difference between actuator and target temperature remains even after the heating time $t_h = 1200$ s. After the heating time, the target temperature is reduced to $\theta_t = 40$ °C for the cool down (for $\theta_t = 70$ °C and $\theta_t = 80$ °C the cool down temperature is set to $\theta_t = 45$ °C). The cooling is clearly visible by a decreasing actuator temperature θ_a. Hereafter, three further cycles can be seen. The described procedure is repeated for the following target temperatures $\theta_t = 60$ °C, 70 °C, 80 °C. Furthermore, the corresponding compression force F is displayed. For $\theta_t = 50$ °C the change in force is minimal, but a clear trend of force F corresponding to the actuator temperature θ_a is visible. For $\theta_t = 60$ °C, the force increases rapidly, following the actuator temperature θ_a. After an increase in force, the gradient of the force graph decreases. The decreasing force gradient is due to the heater band temperature θ_{hb}, which reached the target temperature θ_t and is constant from this moment on. The heat supply is reduced, as the target temperature θ_t only has to be maintained. The steady-state of the heat supply results in the force F approaching a limiting value. The same qualitative behavior can be observed at the actuator temperature θ_a with a time offset. When the cooling starts, a rapid decline in the compression force F and actuator temperature θ_a is observed. The compression force decreases until it reaches a minimum, although the actuator temperature θ_a is decreasing further. The course of the actuator temperature θ_a mainly corresponds to the course of the compression force F. The heating time is chosen in such a way that the compression force F shows a minimal gradient. The temperature distribution in the actuator seems to have reached an almost steady state. Furthermore, the qualitative course of the graph is similar for all cycles and tested temperatures. The heating and cooling rate-limiting factor of the actuator is the thermal conductivity of the paraffin wax. To enhance the reaction or cooling time there are two possibilities. Additives for the paraffin, i.e. copper wool, improve the thermal conductivity within the actuator. Alternatively, the length of the thermal paths within the paraffin wax could be reduced by the integration of thermal conductive structures, i.e. stringers, in the housing. Preliminary investigation confirms the potential of those structures. Therefor these countermeasures are subject of subsequent research.

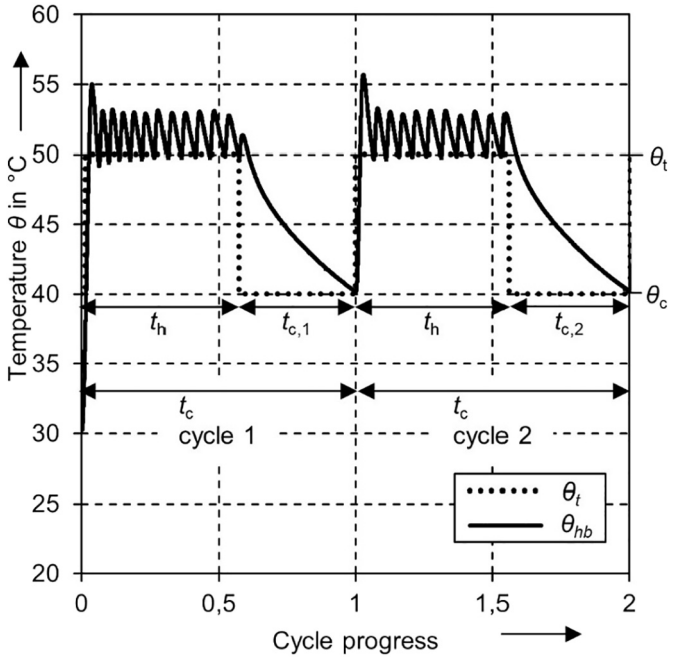

Fig. 8. Example for the test method, two cycles for $h_a = 7$ mm, target θ_t and heater band temperature θ_{hb}.

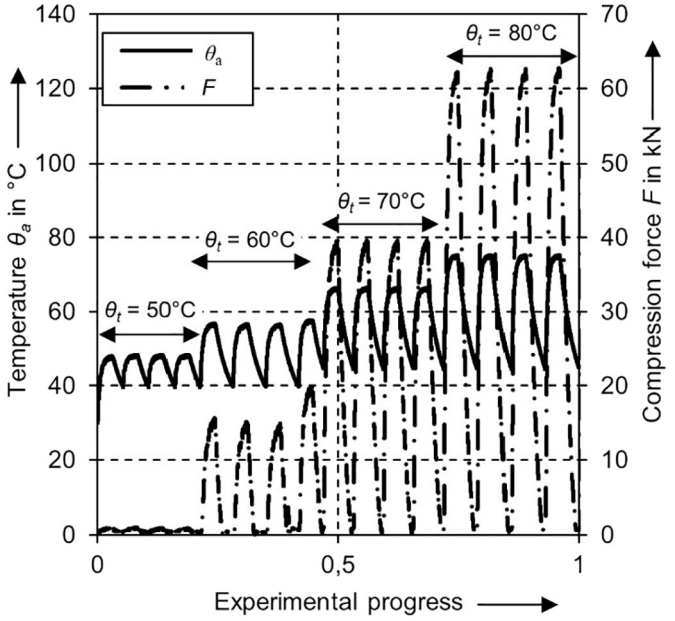

Fig. 9. Complete actuator characterization $h_a = 7$ mm, actuator temperature θ_a and compression force F, the temperature characterization ranges are marked, start-temperature $\theta_0 = 30$ ° C

Table 3 summarizes average maximum forces F_{max} for the tested target temperatures θ_t and standard deviations for all tests. The small standard deviations indicate a good reproducibility. The compression force F increases with increasing θ_t.

Table 3
Summary of the maximum compression forces F_{max}, standard deviations σ and heating times t_h

Temperature θ_t in °C	Average maximum force F_{max} in kN (σ in kN)	Heating time t_h in s
50	0.96 (0.034)	1200
60	16.47 (2.084)	1200
70	39.64 (0.053)	1200
80	62.57 (0.207)	1200

At the temperature $\theta_t = 50$ °C, the melting temperature of paraffin has not been reached yet. Therefore, the volume increase is minimal, resulting in a slight force increase. For the target temperature $\theta_t = 60$ °C a significant increase of the axial force is detectable. In addition, the standard deviation is the highest of all tests. For the first three repetitions, the results are consistent. The fourth repetition shows a significant increase in the force (compare Fig. 9). The target temperature $\theta_t = 60$ °C lies within the melting temperature of the paraffin wax. Obviously, the steady-state of the temperature distribution in the paraffin wax has not yet been set during the first three cycles using $\theta_t = 60$ °C. An increasing temperature and a progressive melting of the paraffin wax explain the increase in force. $\theta_t = 70$ °C and $\theta_t = 80$ °C continue to display an increasing compression force F. At $\theta_t = 70$ °C, the actuators show the same behavior as with lower temperatures but at a higher force level. At $\theta_t = 80$ °C, the actuator reaches the maximum compression force with nearly $F_{max} = 63$ kN.

All prior described tests are performed with a suppressed actuator displacement. In the final test, the effect of an actuator displacement is investigated (Fig. 10). An actuator ($h_a = 7$ mm) is heated for $t = 1200$ s to reach the target temperature θ_t. The compression test machine initiates a displacement of $w = 0.1$ mm in direction of action of force with 0.01 mm/s followed by a change in direction returning to $w = 0.0$ mm using the same speed and recording the compression force F. Due to the optical displacement control an influence of a frame deflection can excluded. The actuator is heated for the next $t = 1200$ s to reach the next target temperature θ_t and the described displacement procedure is repeated. For $\theta_t = 50$ °C, the displacement of $w = 0.1$ mm leads to a complete unloading of the actuator with a resulting compression force $F = 50$ N after the displacement cycle is completed. For $\theta_t = 60$ °C, a decreasing compression force for an increasing displacement is observed. The compression force shows a nearly linear decrease from $F = 11.8$ kN to $F = 4.7$ kN. The change in testing direction leads to an increasing compression force resulting in $F = 13.6$ kN for $w = 0.0$ mm. The start and end displacements show a difference in the compression force. Thus, the graph shows a hysteresis. The target temperatures $\theta_t = 70$ °C and $\theta_t = 80$ °C show similar results, whereby higher target temperatures lead to an increasing difference of the compression force at the start and end of the displacement. When the starting point of the displacement cycle is reached, the axial force decreases at a constant temperature until it is equal to the applied force before the displacement. Furthermore, the graph shows a nonlinear slope. The displacement measurement has a standard deviation of $\Delta w_{dev} = 0.00044$ mm ($\Delta w_{min} = -0.00150$ mm, $\Delta w_{max} = 0.00054$ mm), whereas an influence of acceleration and deceleration processes of the compression test machine cannot be excluded. The hysteresis may be induced by a temperature increase due to the compression, which cannot be measured with the given set-up. Therefore, the hysteresis is not necessarily linked to the actuator or paraffin wax behavior, whereas the literature suggests a temperature dependent hysteresis behavior of paraffin wax [35].

Relaying on the work density defined by Krulevitch et al. it is possible to evaluate the efficiency of the actuator concept. For this purpose, the maximum determined actuating force F at a displacement w of 0.1 mm is compared to the paraffin filling volume V of the actuator. The volume of the paraffin filling is determined by the geometric parameters of the actuator housing (see Fig. 3 and Table 1). The volume of the paraffin core of the actuator is $V = 2845$ mm^3, with the deflection of $d = 0.1$ mm and a maximum force at this point of $F = 37.5$ kN, the working density is calculated as follows.

$$W_d = \frac{F_{max} d_{max}}{2} \frac{1}{V} = \frac{37500\ \mathrm{N} * 0.1\ \mathrm{mm}}{2} \frac{1}{2845\ mm^3} = 659\ \mathrm{J}/m^3 \qquad (2)$$

In relation with the work densities presented by Ogden for known phase-change-material actuators, the presented actuator concept shows a considerable increase in the achievable work density. In comparison to the strongest actuators mentioned (compare [34]) using the membrane principle, an increase by a factor of 7 was achieved. Even in comparison with the structurally stiffer actuators in piston design (compare [30]), an increase by a factor of 2.5 can be achieved.

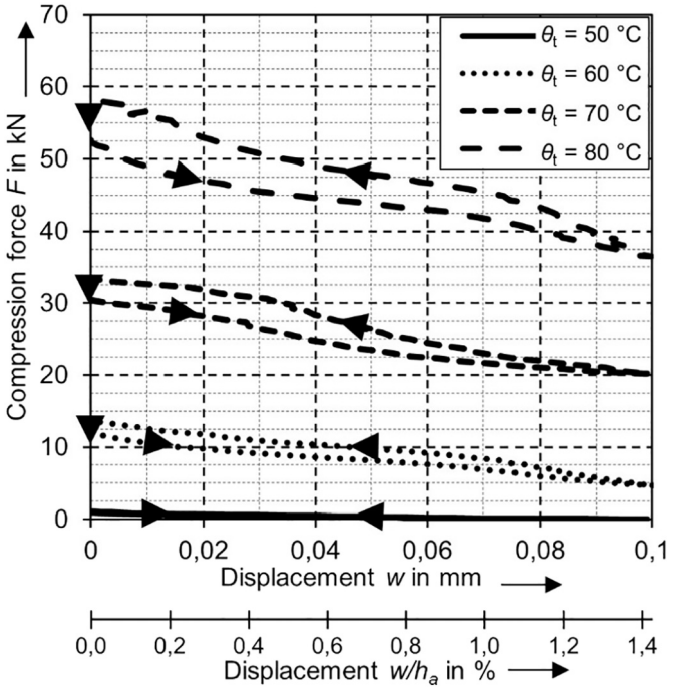

Fig. 10. Compression force displacement diagram for the actuator height $h_a = 7$ mm. The maximum displacement is reached with a velocity of $w = 0,01$ mm/s.

Based on the force displacement characterization, an estimation of the actuators ideal efficiency is possible, as shown in Table 4. The work of the actuators is determined by integrating the compression force F over the displacement w. It is compared with the required amount of heat to warm the paraffin wax up to θ_t. The heat quantity results from the filling volume, the paraffin's specific and latent heat,[1] the housing's specific heat during the heating from $\theta_0 = 27$ ° C at θ_t. The assembly condition and thermal isolation determine the divergence to the estimated efficiency. In comparison with typical data of thermal actuators it is noticeable, that the actuators efficiency increases with higher temperatures and subsequently higher loads. Furthermore, the actuators efficiency reaches at $\theta_t = 80$ ° C the upper limit of reported efficiency of thermal expansion actuators [38]. The efficiency further increases with higher temperatures θ_t.

Table 4
Efficiency characteristic for the actuator with different temperatures θ_t

Temperature θ_t in °C	Positioning work W in Nm	Minimum heat quantity E in J	Actuators efficiency η in [−]
50	0.035	430.4	0.008%
60	0.81	1129.2	0.072%
70	2.43	1708.8	0.142%
80	4.43	1838.0	0.241%

4. Application of a thermal compensation element

The applicability of the described actuator concept is demonstrated in this section. It illustrates the functionality of a paraffin actuator as a passive element, i.e. a compensating element without separate energy supply.

[1] The specific heat of the paraffin used was determined by dynamic differential calorimetry as proposed by Schimmelpfennig et al. [36]. The paraffins latent heat is measured by Schaerer et al. [37].

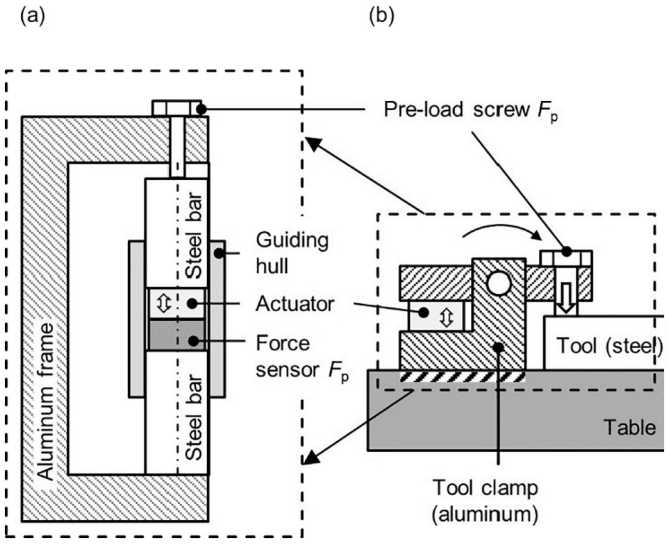

Fig. 11. Test set-up for investigating the thermal compensation of pre-loads (a), application scenario for the actuator in a tool-clamping situation in manufacturing machines (b)

As mentioned before, tool clamping has a significant influence on the result of manufacturing processes [7]. In many cases, the perpetuation of the pre-stress of a clamping under variation of the thermal conditions is required (Fig. 11 b). In an experimental setup, a typical situation is emulated by a frame combining different materials having different coefficients of thermal expansion (Fig. 11 a). The paraffin wax actuator is integrated to compensate this difference in thermal expansion of the materials and therefore to maintain the pre-stress of the system (Fig. 11 a).

A pre-loaded screw introduces a pre-stressing between an aluminum frame and a steel bar. A load cell captures the generated pre-load F_p. As the thermal expansion coefficient of aluminum is approximately twice the thermal expansion coefficient of steel [39], a homogenous heating of the structure without an actuator results in a decreasing pre-load of the system (Fig. 12).

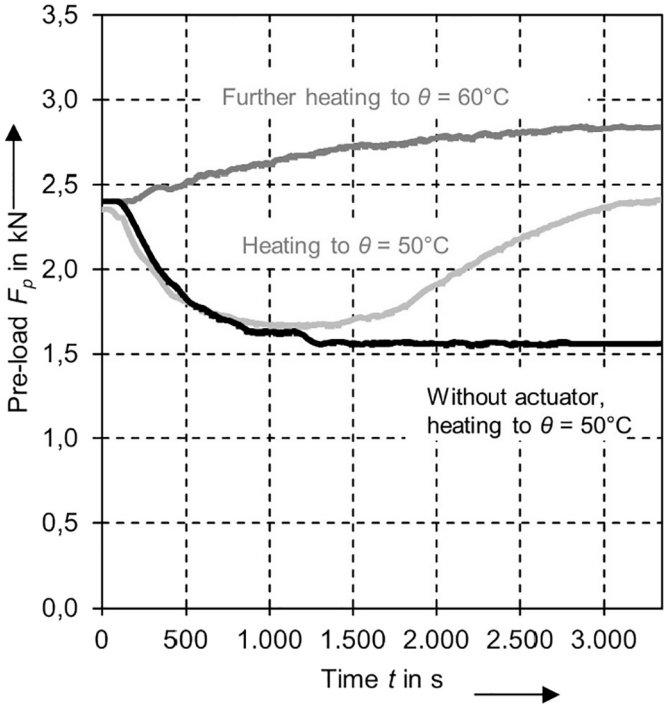

Fig. 12. Pre-load compensation for an aluminum-steel combination placed in an oven in comparison to the same setup without an actuator

Fig. 12 shows the results for a pre-load of $F_p = 2.5$ kN. In accordance with the discussion above, the set-up without an actuator shows a decreasing pre-load with increasing temperature. At about 1500 s, the minimum pre-load for an oven temperature of $\theta = 50$ °C is reached with $F_p = 1.5$ kN. In the second trial, a paraffin wax actuator is placed in the flux of force and is pre-loaded with $F_p = 2.5$ kN. As previously seen, the pre-load is decreasing until 1000 s in the oven at $\theta = 50$ °C. However, after this point in time the paraffin wax inside the actuator starts to melt and thus the pre-load is recovering to $F_p = 2.5$ kN. The decrease of pre-load, initiated by the deviant thermal behavior of aluminum and steel is compensated. The delayed thermal compensation is due to the thermal isolation by the guiding hull (Fig. 11 a). In a third trial the oven temperature is set to $\theta = 60$ °C, which leads to an increase in pre-load of nearly $F_p = 2.8$ kN in addition to the thermal compensation. The results show that the properties of a passive paraffin wax actuator can be adapted to various scenarios.

5. Conclusion

This paper presents a solution to tackle the special challenges in upscaling paraffin wax actuators. The actuator concept fulfills the requirements of a space and cost-efficient actuator that provides high stroke forces. A manufacturing process that serves the challenging joining process is presented; it provides a solid and dense, high-strength connection without melting the phase change material core of the actuator.

The investigations carried out show that the presented compact actuator design enables to apply high forces typically acting in manufacturing devices for clamping and adjustment tasks. Therefore, machinery property adjustments can be performed with paraffin wax actuators. The exhibited sheet metal structure consists of a cutting seal and a metallurgical welded joint. Forces of almost 63 kN can be achieved with an actuator with the diameter of 30 mm and the height $h_a = 7$ mm. The temperature-dependent behavior of the actuator with blocked axial expansion was recorded. The highest tested temperature is $\theta_t = 80$ °C. A further increase in temperature would probably result in a further increase in force. In turn, the actuator forces are limited by the rigidity and strength of the actuator housing. Furthermore, the compression force displacement diagram for the actuator of the height $h_a = 7$ mm is recorded. Even if an actuator displacement of $w = 0.1$ mm is employed, a compression force of $F = 37.5$ kN can still be reached, though a hysteresis occurs. The comparison of the developed actuator concept with existing actuators in membrane design by means of the work density indicator shows an increase in power density by the factor 7.

Finally, the actuator is integrated into an application scenario, which shows the potential of the new actuator concept.

Data availability

The raw/processed data required to reproduce these findings are available from the corresponding author upon reasonable request.

Author contribution

As being the authors of this research paper, we declare that the work is entirely original, any raw data exiting in the article can be provided. Besides, the work has never been submitted/published in any other journal.

Authors' individual contributions

1. Arne Mann: Execution and processing of the experimental investigations and results
2. Thiemo Germann: Processing of the experimental results
3. Mats Ruiter: Execution and evaluation of welding tests
4. Prof. Dr.-Ing. Dipl.-Wirtsch.-Ing. Peter Groche: Supervision of the research, revision of the publication

CRediT authorship contribution statement

Arne Mann: Investigation. **Thiemo Germann:** Validation. **Mats Ruiter:** Investigation. **Peter Groche:** Supervision, Writing - review & editing.

Declaration of competing interest

The authors declare that they have no known competing financial interests or personal relationships that could have appeared to influence the work reported in this paper.

Acknowledgements

The authors want to express their gratitude to the DFG (Deutsche Forschungsgemeinschaft) for the support of the grand “Design methods for novel, energy-efficient, closed phase change actuators with high action of force” (GR 1818/65-1).

References

[1] D.Y. Yang, M. Bambach, J. Cao, J.R. Duflou, P. Groche, T. Kuboki, A. Sterzing, A.E. Tekkaya, C.W. Lee, Flexibility in metal forming, CIRP Ann. 67 (2018) 743–765, https://doi.org/10.1016/j.cirp.2018.05.004.
[2] Hohmann, J.; Schatz, T.; Groche, P. Intelligent wear identification based on sensory inline information for a stamping process. In Proceedings of 5th International Conference on Advanced Manufacturing Engineering and Technologies: NEWTECH 2017; Majstorovic, V., Jakovljevic, Z., Eds.; Springer International Publishing: Cham, s.l., 2017; pp 285–295, ISBN 978-3-319-56429-6.
[3] W. Volk, P. Groche, A. Brosius, A. Ghiotti, B.L. Kinsey, M. Liewald, L. Madej, J. Min, J. Yanagimoto, Models and modelling for process limits in metal forming, CIRP Ann. (2019) https://doi.org/10.1016/j.cirp.2019.05.007.
[4] J.M. Allwood, S.R. Duncan, J. Cao, P. Groche, G. Hirt, B. Kinsey, T. Kuboki, M. Liewald, A. Sterzing, A.E. Tekkaya, Closed-loop control of product properties in metal forming, CIRP Ann. 65 (2016) 573–596, https://doi.org/10.1016/j.cirp.2016.06.002.
[5] P. Groche, F. Hoppe, T. Kessler, A. Kleemann, Industrial Working Environment 2025. NEBU 2018: Neuere Entwicklungen in der Blechumformung, 2018.
[6] T. Bäume, W. Zorn, W.-G. Drossel, G. Rupp, Iterative process control and sensor evaluation for deep drawing tools with integrated piezoelectric actuators, Manufacturing Rev 3 (2016) 3, https://doi.org/10.1051/mfreview/2016002.
[7] D. Kraus, M. Lieberenz, P. Groche, Reduction of tool wear by systematic design of the tool clamping situation, J. Manuf. Process. 28 (2017) 449–456, https://doi.org/10.1016/j.jmapro.2017.04.011.
[8] K. Wegener, J. Mayr, M. Merklein, B.-A. Behrens, T. Aoyama, M. Sulitka, J. Fleischer, P. Groche, B. Kaftanoglu, N. Jochum, et al., Fluid elements in machine tools, CIRP Ann. 66 (2017) 611–634, https://doi.org/10.1016/j.cirp.2017.05.008.
[9] P. Zoller, D.J. Walsh, Standard pressure-volume-temperature data for polymers, Technomic Publ, Lancaster, 1995, ISBN 1566763282.
[10] S. Ogden, L. Klintberg, G. Thornell, K. Hjort, R. Bodén, Review on miniaturized paraffin phase change actuators, valves, and pumps, Microfluid. Nanofluid. 17 (2014) 53–71, https://doi.org/10.1007/s10404-013-1289-3.
[11] A. Mann, C. Bürgel, P. Groche, A modeling strategy for predicting the properties of paraffin wax actuators, Actuators 7 (2018) 81, https://doi.org/10.3390/act7040081.
[12] H. Mehling, L.F. Cabeza, Heat and Cold Storage with PCM. An up to Date Introduction into Basics and Applications; with 28 Tables, Springer, Berlin, Heidelberg, 2008.
[13] Y. Jin, Q. Wan, Y. Ding, PCMs heat transfer performance enhancement with expanded graphite and its thermal stability, Procedia Engineering 102 (2015) 1877–1884, https://doi.org/10.1016/j.proeng.2015.01.326.
[14] C. Chen, Z. Huang, Y. Jiao, L.-A. Shi, Y. Zhang, J. Li, C. Li, X. Lv, S. Wu, Y. Hu, et al., In situ reversible control between sliding and pinning for diverse liquids under ultra-low voltage, ACS Nano 13 (2019) 5742–5752, https://doi.org/10.1021/acsnano.9b01180.
[15] M.D. Lima, N. Li, M. Jung de Andrade, S. Fang, J. Oh, G.M. Spinks, M.E. Kozlov, C.S. Haines, D. Suh, J. Foroughi, et al., Electrically, chemically, and photonically powered torsional and tensile actuation of hybrid carbon nanotube yarn muscles, Science 338 (2012) 928–932, https://doi.org/10.1126/science.1226762.
[16] K.-Y. Chun, S. Hyeong Kim, M. Kyoon Shin, C. Hoon Kwon, J. Park, Y. Tae Kim, G.M. Spinks, M.D. Lima, C.S. Haines, R.H. Baughman, et al., Hybrid carbon nanotube yarn artificial muscle inspired by spider dragline silk, Nat. Commun. 5 (2014) 3322, https://doi.org/10.1038/ncomms4322.
[17] S.M. Mirvakili, I.W. Hunter, Artificial muscles: mechanisms, applications, and challenges, Adv. Mater. Weinheim. 30 (2018) https://doi.org/10.1002/adma.201704407.
[18] D. Sangian, J. Foroughi, S. Farajikhah, S. Naficy, G.M. Spinks, A bladder-free, non-fluidic, conductive McKibben artificial muscle operated electro-thermally, Smart Mater. Struct. 26 (2017), 15011. https://doi.org/10.1088/1361-665X/26/1/015011.
[19] . Vernet, S. Sealing Means. US2368181A, Jan 30, 1945.
[20] J.F. Sherwood, Devices for Utilizing the Thermal Expansion of Wax. US2815642A, Dec 10, 1957.
[21] S. Tibbitts, High output paraffin actuators: Utilization in aerospace mechanisms, The 22nd Aerospace Mechanisms Symposium, NASA. Langley Research Center 1988, pp. 13–28.
[22] N. Kabei, M. Kosuda, H. Kagamibuchi, R. Tashiro, H. Mizuno, Y. Ueda, K. Tsuchiya, A thermal-expansion-type microactuator with paraffin as the expansive material. (basic performance of a prototype linear actuator): basic performance of a prototype linear actuator, JSME Int. J. Ser. C Mech. Syst. Mach. Elem. Manuf. 40 (1997) 736–742, https://doi.org/10.1299/jsmec.40.736.
[23] Behr Thermot-tronik GmbH, Dehnstoffarbeitselemente: Produktkatalog Behr Thermot-tronik, GmbH, 2014.
[24] L. Klintberg, M. Karlsson, L. Stenmark, J.-Å. Schweitz, G. Thornell, A large stroke, high force paraffin phase transition actuator, Sensors Actuators A Phys. 96 (2002) 189–195, https://doi.org/10.1016/S0924-4247(01)00785-3.
[25] L. Klintberg, M. Karlsson, L. Stenmark, G. Thornell, A thermally activated paraffin-based actuator for gas-flow control in a satellite electrical propulsion system, Sensors Actuators A Phys. 105 (2003) 237–246, https://doi.org/10.1016/S0924-4247(03)00203-6.
[26] E.T. Carlen, C.H. Mastrangelo, Electrothermally activated paraffin microactuators, J. Microelectromech. Syst. 11 (2002) 165–174, https://doi.org/10.1109/JMEMS.2002.1007394.
[27] R. Bodén, M. Lehto, U. Simu, G. Thornell, K. Hjort, J.-Å. Schweitz, A polymeric paraffin actuated high-pressure micropump, Sensors Actuators A Phys. 127 (2006) 88–93, https://doi.org/10.1016/j.sna.2005.11.068.
[28] S. Svensson, G. Sharma, S. Ogden, K. Hjort, L. Klintberg, High-pressure peristaltic membrane micropump with temperature control, J. Microelectromech. Syst. 19 (2010) 1462–1469, https://doi.org/10.1109/JMEMS.2010.2076784.
[29] M. Lehto, Paraffin Actuators in Microfluidic Systems, Acta Universitatis Upsaliensis Acta Universitatis Upsaliensis, Uppsala, 2007 (978-91-554-6942-9).
[30] R. Bodén, Microactuators for Powerful Pumps, Acta Universitatis Upsaliensis, Uppsala, 2008, ISBN 978-91-554-7352-5.
[31] J.S. Lee, S. Lucyszyn, Bulk-Mikromachined hydraulic microactuator, in: C.-J. Sun (Ed.), Science and Technology of Hybrid Materials, ICMAT 2005, IUMRS-ICAM 2005: Proceedings of Symposium S Science and Technology of Hybrid Materials (ICMAT 2005), 3–8 July 2005 Singapore: The 3rd International Conference on Materials for Advanced Technologies: International Union of Materials Research Societies' 9th International Conference on Advanced Materials, Trans Tech Publications: Uetikon-Zuerich, United Kingdom, 2010.
[32] P. Krulevitch, A.P. Lee, P.B. Ramsey, J.C. Trevino, J. Hamilton, M.A. Northrup, Thin film shape memory alloy microactuators, J. Microelectromech. Syst. 5 (1996) 270–282, https://doi.org/10.1109/84.546407.
[33] J.S. Lee, S. Lucyszyn, Thermal analysis for bulk-micromachined electrothermal hydraulic microactuators using a phase change material, Sensors Actuators A Phys. 135 (2007) 731–739, https://doi.org/10.1016/j.sna.2006.07.033.
[34] S. Ogden, R. Bodén, K. Hjort, A Latchable valve for high-pressure microfluidics, J. Microelectromech. Syst. 19 (2010) 396–401, https://doi.org/10.1109/JMEMS.2010.2041749.
[35] B.-y. Chen, Y. Liu, X.-h. Zhang, C.-c. Sun, Study on Influence Factors of Thermal Hysteresis in Paraffin Actuator, 2008 1145–1148, https://doi.org/10.1109/ICICTA.2008.272.
[36] M. Schimmelpfennig, K. Weber, F. Kalb, K.-H. Feller, T. Butz, M. Matthäi, Volumenausdehnung von Paraffinen aus Steigrohr-Messungen, 2007.
[37] A.A. Schaerer, C.J. Busso, A.E. Smith, L.B. Skinner, Properties of pure normal alkanes in the C 17 to C 36 range, J. Am. Chem. Soc. 77 (1955) 2017–2019, https://doi.org/10.1021/ja01612a097.
[38] J.E. Huber, N.A. Fleck, M.F. Ashby, The selection of mechanical actuators based on performance indices, Proc. R. Soc. Lond. A 453 (1997) 2185–2205, https://doi.org/10.1098/rspa.1997.0117.
[39] VDI-Wärmeatlas, *Mit 320 Tabellen;* Gesellschaft Verfahrenstechnik und Chemieingenieurwesen, 11., bearb. und erw. Aufl, Springer Vieweg, Berlin, 2013, ISBN 978-3-642-19981-3.